Journal of the Physical Society of Japan
Vol. 62, No. 10, October, 1993, pp. 3661-3679

STM Study of Anisotropic Superconducting Gap of $Bi_2Sr_2CaCu_2O_8$

Koichi ICHIMURA and Kazushige NOMURA

Department of Physics, Hokkaido University, Sapporo 060

(Received March 15, 1993)

The electron tunneling study was carried out on $Bi_2Sr_2CaCu_2O_8$ with use of the scanning tunneling microscope. Both the cleaved and lateral surface of single crystal were investigated. The electronic density of states for the superconducting phase was correctly obtained at the lateral surface. It shows the finite gap on the whole Fermi surface clearly, while the gap has a considerable anisotropy. The temperature dependence of the magnetic field penetration depth was also measured and its thermally activated behavior confirmed the finite gap again. These results indicate the large *s*-wave component in the pair wave function and the fair contribution of *d*-wave as well. The attractive force between electrons is not only due to the on-site interaction, but also the extended one.

[Bi-based cuprate superconductor, STM spectroscopy, anisotropic superconducting gap, penetration depth, pairing symmetry]

§1. Introduction

Since the discovery of high transition temperature T_c superconductivity in $La_{2-x}Ba_xCuO_4$,[1] cuprate superconducting oxides with higher T_c have been found in succession. A lot of interests have been taken in the origin of extremely high transition temperature. The mechanism of superconductivity is explained by the BCS theory[2] in conventional superconductors, in which electron pairs so-called Cooper pairs formed through the attractive force mediated by the electron-phonon interaction play an essential role. According to the BCS theory, T_c is given in the weak-coupling limit as

$$kT_c=\hbar\omega_D \exp(-1/N(0)V), \qquad (1)$$

where ω_D is the Debye frequency, $N(0)$ is the electronic density of states at the Fermi level and V is the strength of the attractive interaction due to the electron-phonon interaction. For strong-coupling superconductors, McMillan predicted that T_c is at most 40 K.[3] Observed T_c in cuprate superconductors is much higher beyond such a prediction. Other pairing mechanism than the attractive force mediated by phonon is expected.

The symmetry of the pair wave function is directly connected with the symmetry of the attractive force. The Cooper pair in the BCS superconductor is of the spin singlet state and the orbital part of the pair wave function has the *s*-wave symmetry. In investigating the origin of the attractive force, it is important to clarify the symmetry of the pair wave function. In the NMR measurement,[4] the Knight shift was observed to decrease rapidly below T_c, and indicated that the electron pair is also of the spin singlet state in cuprate superconductors as well. Accordingly the symmetry with even parity, *e.g. s* and *d*-wave, is allowed for the pair wave function.

In cuprate superconductors, metallic conduction is mainly born by holes doped in oxygen $2p_\sigma$ orbital, strongly hybridized with Cu $3d_{x^2-y^2}$,[5] within the Cu-O layer. The on-site Coulomb interaction V_C on Cu site is strong ($V_C \sim 6$ eV)[5,6] and the nearly half filled band favors that localized spins at Cu site are arranged in anti-ferromagnetic order. In this strong correlation system, it is suspected to be difficult to form electron (hole) pairs by the on-site attractive force, which is presumably cancelled out by the large Coulomb repulsive force. The attractive interaction with the *d*-wave symmetry would be a possible candidate for the origin of superconductivity in such a

strong correlation system. In the heavy fermion system with the strong correlation, the temperature dependence of nuclear spin-lattice relaxation rate $1/T_1$,[7] specific heat[8] and magnetic field penetration depth[9] suggest a gapless nature. It is considered that the *d*-wave symmetry paring is realized. In cuprate superconductors as well, the temperature dependence of $1/T_1$ showing a gapless nature was reported[10] for $YBa_2Cu_3O_7$; the enhancement just below T_c (coherence peak) was not found and the temperature dependence below T_c follows the power law. On the other hand, the temperature dependence of the penetration depth $\lambda(T)$ of $YBa_2Cu_3O_7$[11] is well fitted by the BCS local limit equation and suggests the *s*-wave pairing. In such a present controversial situation, it is very important to clarify the pairing symmetry closely connected with the origin of the attractive force.

In this article, the electron tunneling spectroscopic investigation on single crystals of $Bi_2Sr_2CaCu_2O_8$ with use of Scanning Tunneling Microscope (STM) is described. The purpose of this study is to clarify the mechanism of high-T_c superconductivity, particularly the symmetry of the pair wave function from the electronic density of states in the superconducting phase. In addition, the temperature dependence of the penetration depth was also investigated to confirm the result of the tunneling spectroscopy. In §2, the background of this study is briefly described. The tunneling spectroscopic measurement was performed both at the cleaved and lateral surface of single crystal. Both results are described in §4.1 and §4.2, respectively. The result of the temperature dependence of the penetration depth is described in §4.3. The symmetry of the pair wave function is discussed in §5.

§2. Tunneling Spectroscopy and High-T_c Superconductor

2.1 Tunneling spectroscopy with STM

The electron tunneling spectroscopic method is the most direct method for investigation of the electronic density of states. The existence of the energy gap in the superconducting ground state predicted by the BCS theory has been directly proven by the pioneer electron tunneling measurement.[12] The evidence for the pairing mediated by the electron-phonon interaction was also provided by the tunneling spectroscopy.[13] The electron tunneling method is one of the most useful techniques in investigation of the mechanism of superconductivity.

The tunnel junction method or the point-contact method have been widely used until the invention of STM (Scanning Tunneling Microscope). The first STM measurement demonstrated its usefulness in the direct observation of Si reconstructed surface in the real space.[14] The STM method is based on the electron tunneling between the sample surface and the non-contacting counter-electrode (tunneling tip). Because the tip is separated by vacuum from sample surface, the STM method provides less disturbance to the electronic state in the sample as compared with former two methods, in which the counter-electrode contacts directly with the sample. In the STM the tip is approached to the sample surface about less than 1 nm and the electron tunneling occurs through the restricted area containing a few atoms at most. Uncertainty of the wave number is estimated as $1/a \sim k_F$ with the lattice constant a and the Fermi wave number k_F. The wave number of tunneling electron is, accordingly, no longer conserved in each tunneling process. Therefore, the tunneling current in the STM method is given as a total sum of every wave number components. Because of its non-contacting tip and locality, the STM can probe local electronic states. The structure of Charge Density Wave (CDW) was successfully observed in the real space.[15] The sliding motion of CDW at the surface in $K_{0.3}MoO_3$ was investigated directly.[16] The observation of the flux lattice in $NbSe_2$[17] proved that the STM is very useful to investigate the local electronic state for the superconducting phase.

The tunneling current I is most simply given as a function of the distance d between the tip and the sample surface as,

$$I = I_0(V) \exp(-d/d_0), \tag{2}$$

where $I_0(V)$ is the characteristic current determined by the bias voltage V applied between the tip and the sample, and the length d_0 is the parameter which characterizes the extension of electronic wave function of the tip material

and the sample. According to above relation, the tip distance is controlled by the tunneling current for a constant bias voltage; with increasing the tunneling current, the tip distance becomes narrow. In the simple tunneling theory, the characteristic current $I_0(V)$ in eq. (2) is given as a function of the bias voltage V as

$$I_0(V) \propto \int_{-\infty}^{+\infty} |M(E, E+eV)|^2 N_t(E) N_s(E+eV)\{f(E)-f(E+eV)\}\, dE, \quad (3)$$

where N_t and N_s are the electronic densities of states for the tip metal and the sample, respectively. Here only the energy conservation is considered, because the wave number is not conserved in the STM method as described before. The tunneling matrix element denoted by $|M|$ is usually assumed to be independent of the energy of tunneling electron E. If N_t is constant with respect to E, we obtain the well-known equation for absolute zero temperature as

$$dI/dV \propto N_s(eV). \quad (4)$$

Since the electron tunneling occurs at a restricted area containing at most a few atoms near the tip in the STM method, one can also study the local density of states of the sample surface with varying the tip position.

2.2 *Tunneling spectroscopy on high-T_c superconductors*

A lot of electron tunneling measurements have been done on high-T_c cuprate superconductors up to the present. Reported values of the gap parameter Δ are much larger than the BCS prediction for the weak-coupling limit and it is suggested that high-T_c oxides are the strong-coupling superconductor. In early stage of the tunneling investigation, obtained values for $2\Delta/kT_c$ showed a wide scatter; La-Sr-Cu-O ($2\Delta/kT_c$=4.5-9),[18] Y-Ba-Cu-O (3-4),[19] Nd-Ce-Cu-O (5),[20] Tl-Ba-Ca-Cu-O (4),[21] Bi-Sr-Ca-Cu-O (5-11).[22-26] Recently, high quality samples have been grown and used for the tunneling measurement. Consequently, reproducible results have been obtained. As a result, the value of $2\Delta/kT_c$ tends to converge; *e.g.* $2\Delta/kT_c$ is obtained reliably about 7 for Bi-Sr-Ca-Cu-O. However, the precise shape of the tunneling conductance curve is still different from experiment to experiment.

At present, main interest moves rather to elucidating the mechanism of high-T_c superconductivity than the value of Δ. The phonon structure as observed in conventional strong-coupling superconductors was reported[25] in $Bi_2Sr_2CaCu_2O_8$. However, the whole shape of the tunneling conductance shows an extraordinary so-called V-shape and moreover the conductance in the normal phase is not observed precisely. The claim that the attractive force is mediated by the electron-phonon interaction is not conclusive. Although the possibility of the anisotropic gap was pointed out, the symmetry of the pair wave function was not established yet.

The STM study has been done vigorously in Bi-Sr-Ca-Cu-O, where the clean surface can be obtained easily by the cleavage. The spatial variation of the gap parameter was found.[23,26] The tip distance dependence of the tunneling conductance curve obtained at the cleaved surface was also reported.[27-29] This suggests that under some condition the tunneling differential conductance is no more proportional precisely to the electronic density of states for the superconducting phase. It is worth noting that one should examine results of the tunneling spectroscopy on high-T_c cuprate superconductors with a layered structure, with great care, as described in §4.1.3.

2.3 *Penetration depth measurement*

The Meissner effect is another phenomenon characterizing the superconducting state. The magnetic field penetration depth $\lambda(T)$ is inversely proportional to the square root of the number of electrons condensed in the superconducting phase. Therefore, the temperature dependence of the penetration depth is sensitive to the quasi-particle excitation which is directly connected with the electronic density of states in the superconducting phase $N(E)$. The penetration depth $\lambda(T)$ is given simply as

$$\frac{\lambda(T)}{\lambda(0)}=\left[1-2\int_0^{+\infty}\left(-\frac{\partial f}{\partial E}\right)N(E)\,dE\right]^{-1/2}, \tag{5}$$

where f denotes the Fermi distribution function. The integral in large bracket corresponds to the number of excited quasi-particles.

If the gap is finite everywhere on the Fermi surface as in the case of the BCS superconductor, the finite energy is needed for the excitation of quasi-particles. The temperature dependence of $\lambda(T)-\lambda(0)$ would be a thermal activation type; i.e. $\lambda(T)$-$\lambda(0)$ varies as $\exp(-\Delta/kT)$ at low temperature region ($kT \ll \Delta$). On the other hand, if the gap vanishes somewhere on the Fermi surface, quasi-particle can be excited with infinitesimal energy and the power law behavior is expected for $\lambda(T)-\lambda(0)$ instead. If Δ vanishes at points on the Fermi surface, the electronic density of states is proportional to E^2 at low energy region. This leads to T^2 dependence of $\lambda(T)-\lambda(0)$. If Δ vanishes along lines on the Fermi surface, the electronic density of states proportional to E leads to T-linear dependence. Therefore, from the temperature dependence of the penetration depth, we can know whether the energy gap is finite on the Fermi surface or vanishes at points or lines.

In cuprate superconductors, the penetration depth has been investigated by magnetization measurements,[11,30-32] μSR measurements,[33,34] etc. For $Bi_2Sr_2CaCu_2O_8$, Harshman *et al.*[34] reported that the temperature dependence of the penetration depth is consistent with the empirical Gorter-Casimir law from the μSR measurement. For $YBa_2Cu_3O_7$, the thermal activated behavior was reported both from the magnetization measurement[11,30] and the μSR measurement.[33] These results support that the pair wave function is of the s-wave symmetry in cuprate superconductors. However, Maeda *et al.*[32] reported T^2 dependence from the rf-resonance method for $Bi_2Sr_2CaCu_2O_8$.

§3. Experimental

3.1 Sample

The crystal structure of $Bi_2Sr_2CaCu_2O_8$ is orthorhombic with $a=0.541$ nm, $b=0.542$ nm and $c=3.09$ nm,[35] as shown in Fig. 1. $Bi_2Sr_2CaCu_2O_8$ has a layered structure consisting of Ca layer sandwiched between two Cu–O, two Sr–O and two Bi–O layers. Single crystals of $Bi_2Sr_2CaCu_2O_8$ were synthesized by the floating-zone method.[36] Many single crystals were grown sticking together. After separating them, most crystals showed cleaved surfaces of the Bi–O layer (the *a-b* plane) and rough side surfaces. In rare cases, the extremely clean lateral surface appeared. This surface is parallel to the *a*-axis and oblique in the direction of the *b*-axis. This lateral surface looks grey under a optical microscope, while the cleaved Bi–O surface is shiny. Yamanaka *et al.*[37] succeeded to obtain (ZZ) Raman spectra at this lateral surface and confirmed little surface disorder. The typical dimension of such a clean lateral surface area is 0.2×0.2 mm^2. The sample was glued with epoxy adhesive on a thin glass plate parallel to the *a-b* plane of the crystal for the measurement at the cleaved surface. For the measurement at the lateral surface the thin sample was supported with small block. A gold wire of 50 μm diameter was attached to the sample with silver paste for the current lead. A fresh surface was obtained by cleaving with use of adhesive tape immediately before the sample was mounted on the sample

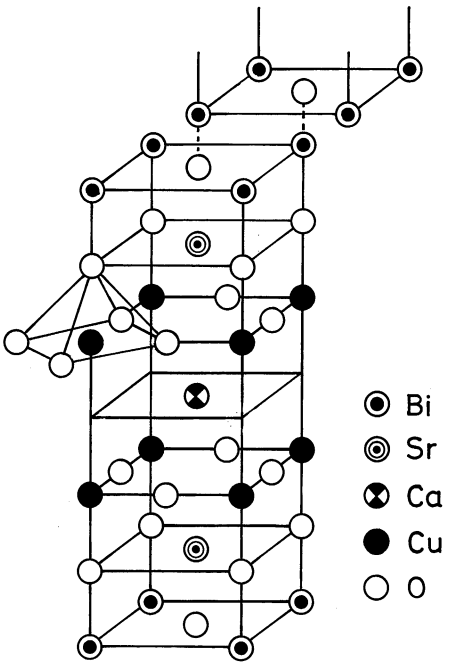

Fig. 1. Crystal structure of $Bi_2Sr_2CaCu_2O_8$.

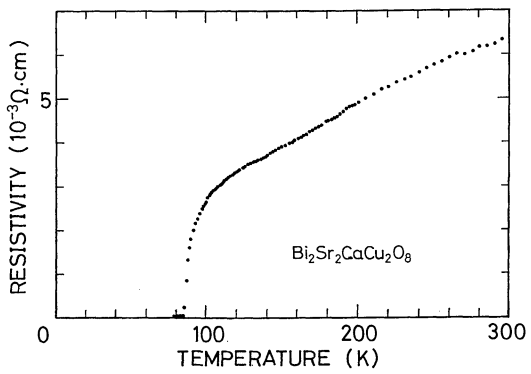

Fig. 2. Temperature dependence of the resistivity of a single crystal of $Bi_2Sr_2CaCu_2O_8$. The superconducting transition temperature T_c is determined as T_c= 87 K from the midpoint of resistive transition.

holder of the STM unit.

Figure 2 shows the temperature dependence of the resistivity measured with four probes configuration after the STM measurement. The superconducting transition temperature T_c was determined as T_c=87 K from the midpoint of the resistive transition.

3.2 *STM measurement*

The main part of the STM unit consists of a scanning tip and a tube type piezoelectric actuator. The vertical position of the sample can be adjusted coarsely by the screw which is operable from the room temperature space. The scanning tip is arranged to be perpendicular to the sample surface and the distance between the tip and the sample is controlled finely by the tube actuator. The vacuum sealed cell containing the STM unit is filled with thermal exchange helium gas to achieve thermal equilibrium and temperature is smoothly controlled in this cell. The cryostat attached with the cell is immersed directly in liquid helium. In order to minimize the external vibration the helium dewar is mounted on a vibration isolator which is equipped with air suspensions. The liquid nitrogen outer dewar is installed on the floor directly. In the present study, a mechanically sharpened thin wire of Pt was used as the scanning tip, the density of states of which is known to vary slowly near the Fermi level. The sharpness of the tip was tested by taking an STM image of graphite surface at room temperature.

The distance between the tip and the sample surface is controlled with the voltage applied to the z-actuator by making the tunneling current I_0 constant for the constant tunneling bias V_0 prior to the voltage sweep in the spectroscopic measurement. During the voltage sweep, the tip distance is kept constant by the constant control voltage to the z-actuator. The tunneling bias was swept in the form of a 15–30 sec triangular wave. AC (0.5–1 kHz) modulation of small amplitude (*e.g.* 0.5 mV peak to peak for $Bi_2Sr_2CaCu_2O_8$) was superimposed to the sweep voltage for the differential detection. The differential conductance was directly obtained as a function of the bias voltage with use of a lock-in amplifier.

In order to check that the sample surface is prevented from a direct contact with the tip, we investigated the reproducibility of the tunneling conductance by varying the tip distance and changing the tip position on the sample surface repeatedly. We confirmed that the $dI/dV-V$ curve at the fixed tip distance and at the fixed position is reproduced repeatedly even after the sweep of the tip on the sample surface. This fact assures that the tip does not contact with the sample surface directly, nor damage the sample. The configuration without direct contact indicates that the tunneling gap is mainly provided with the vacuum gap between the tip and the sample surface.

3.3 *Measurement of the penetration depth*

The penetration depth of the magnetic field is obtained from the magnetic susceptibility of thin plate sample. We measured the magnetization by the AC inductance method. The mutual inductance L_{mut} is obtained by detecting the induced electromotive force between both ends of a pair of counterwound pick-up coils, which is mounted inside the excitation coil, with use of a lock-in amplifier. The sample glued on a teflon rod holder is moved vertically through pick-up coils slowly (about 20 sec for one stroke), the output voltage of a lock-in amplifier is recorded on a X-Y recorder. The signal from the teflon rod is negligible as compared with that of the sample, when the sample is of the superconducting phase. Although the magnetization M is not uniform due to the penetration of the mag-

netic field, here we use the term of the susceptibility χ as $\chi=M/VH$, where V is the volume of the sample and H is the applied field. With use of a dual phase lock-in amplifier we can obtain the real part χ' and the imaginary one χ'' of the complex susceptibility $\chi=\chi'-i\chi''$ simultaneously. Thin plate shaped samples with typical dimension of $1\times2\times0.1$ mm^3 were used in the present measurement. Since the magnetic field was applied parallel to the longer direction of the plate sample, the demagnetization field was quite small. Since the thickness of the present sample d is much small, we assume that the magnetic field penetration perpendicular to the plate (parallel to the c-axis) is dominant. The susceptibility χ' in the superconducting phase is given as

$$-4\pi\chi'=1-\frac{2\lambda}{d}\tanh\frac{d}{2\lambda}. \tag{6}$$

When $d\gg\lambda(T)$,

$$-4\pi\chi'\simeq1-\frac{2\lambda}{d}. \tag{7}$$

Above condition is satisfied except very near T_c. By using eq. (7), the temperature dependence of the penetration depth $\lambda(T)$ is obtained from $\chi'(T)$ as

$$\lambda(T)-\lambda(T_{\min})=-4\pi\left[\frac{2\{\chi'(T)-\chi'(T_{\min})\}}{d}\right], \tag{8}$$

where $T_{\min}$ is the lowest temperature in the measurement.

About 1 kHz AC magnetic field of 0.1–1 G amplitude was applied with the excitation coil. In the range of the field amplitude of 0.1–1 G, the imaginary part χ'' which corresponds to an energy dissipation presumably by the flux motion, could not be detected except near T_c (84 K$<T<$89 K). Additionally, the linearity of M-H curve was also confirmed at 80 K. The $\chi(T)$ curve was identical irrespective of the field amplitude except just below T_c. These assured that the external field did not exceed the lower critical field H_{c1} in almost whole temperature range in the present measurement.

§4. Results and Discussion

4.1 Tunneling at the cleaved surface

4.1.1 Conductance curve at 4.2 K

A typical tunneling $dI/dV-V$ curve at the cleaved Bi–O surface at 4.2 K is shown in Fig. 3. The superconducting gap structure is clearly seen as a dip of differential conductance. As described in detail in §4.1.3, the $dI/dV-V$ curve obtained at the cleaved surface is no longer proportional to the electronic density of states; the shape of the $dI/dV-V$ curve changes depending on the distance between the tip and the sample surface. However, it was confirmed empirically that for the appropriate tip distance, where the conductance at bias voltage $V=150$ mV is about 20 nS, $dI/dV-V$ curves are very similar to the correct density of states in the superconducting phase, which is obtained by the tunneling measurement at the lateral surface as discussed in §4.2 in detail. Therefore, we discuss the spatial variation and the temperature dependence of the gap parameter with results obtained at the cleaved surface under such a condition.

From the short coherence length estimated as the order of a few nm,[38] it is expected that the gap parameter varies within small region. The tunneling conductance at various positions of the sample surface was investigated, details of which are described in our previous

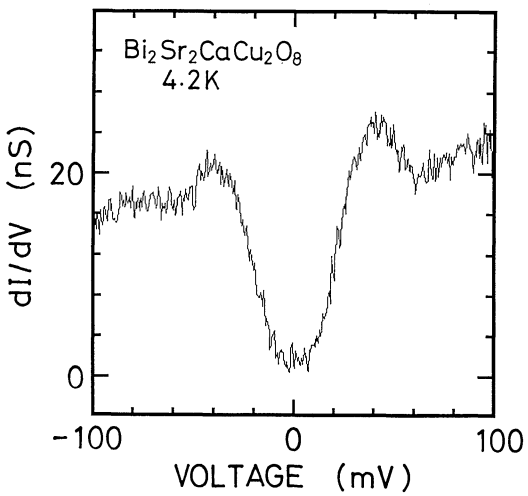

Fig. 3. Typical $dI/dV-V$ curve for the tunneling at the cleaved Bi–O surface at 4.2 K.

article.[26] We found that the curve of $dI/dV-V$ varies in space. The characteristic length of variation of Δ is of the order of 10 nm. Such a short range variation of the gap parameter would be related to the short coherence length a few nm and some inhomogeneity. Vieira *et al.*[23] also found the spatial variation of the superconducting gap at the sample surface of $Bi_4Sr_3Ca_3Cu_4O_{16}$ with the STM. Their result is qualitatively consistent with ours. It should be noted that the spatial variation of Δ is found commonly in different materials. However, it is still now open problem whether such a spatial variation is essential for the mechanism of superconductivity or not.

4.1.2 Temperature dependence of the gap parameter

Curves of $dI/dV-V$ obtained at various temperature are shown in Fig. 4. Each curve is shifted by two divisions. The tip distance was controlled at the initial current $I_0=8$ nA for $V_0=150$ mV. At low temperature, the superconducting energy gap structure is clear and the conductance near zero bias voltage is reduced to almost zero. With increasing the temperature the midgap conductance increases and the structure of the energy gap is gradually smeared out. The superconducting gap structure becomes vague near T_c. However, the broad dip still remains even above T_c. This broad dip disappears above 120 K. We can not determine whether this broad dip is essential in the electronic state of this material or not, because the tunneling conductance measured at the cleaved surface might contain an extrinsic effect as discussed in §4.1.3 in detail. Therefore, we do not discuss the broad dip farther here.

Figure 5 shows the temperature dependence of the gap parameter determined from the fit of the $dI/dV-V$ curve to eq. (9) described in §4.2.2. In the figure, the gap parameter normalized by $\Delta(4.2\text{ K})=26$ meV is plotted as a function of the reduced temperature T/T_c with $T_c=87$ K. When temperature is varied, the small displacement of the tip position at the sample surface is inevitable owing to the thermal expansion of the actuator and the sample holder. In Fig. 5 all the data is plotted irrespective of the tip position at the sample sur-

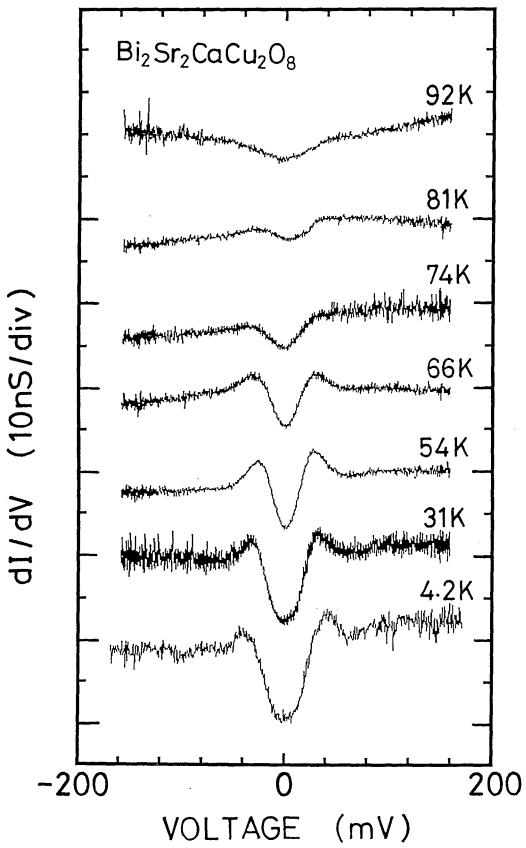

Fig. 4. $dI/dV-V$ curve for the tunneling at the cleaved surface at various temperature. The zero conductance line of each curve is shifted by two divisions for clarity.

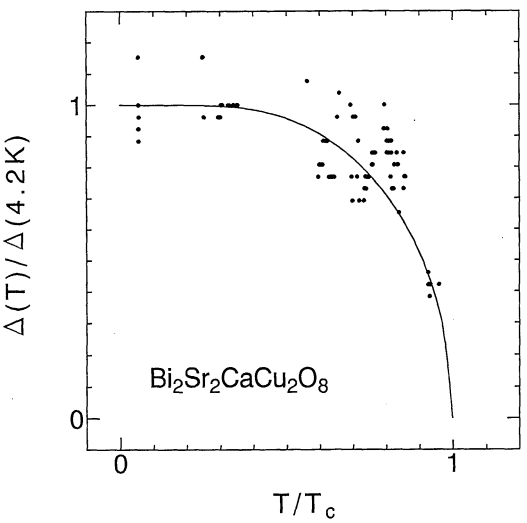

Fig. 5. Normalized gap parameter $\Delta(T)/\Delta(4.2\text{ K})$ as a function of the reduced temperature T/T_c with $\Delta(4.2\text{ K})=26$ meV and $T_c=87$ K. The solid curve shows the BCS prediction.

face. The relatively large scatter in Fig. 5 is partly due to the position dependent Δ value as discussed in §4.1.1. The gap parameter is almost constant at low temperature, and tends to decrease with increasing temperature. The solid line represents the BCS prediction of the isotropic gap with $\Delta(4.2\,\mathrm{K})=26$ meV and $T_c=87$ K. As found in Fig. 5, the temperature dependence of the gap is qualitatively consistent with the BCS theory. However, this does not exclude necessarily the *d*-wave paring, because the temperature dependence of the gap parameter calculated[39] for the *d*-wave symmetry with weak-coupling limit is similar to the BCS prediction. Both *s* and *d*-wave symmetry are allowed from the present result. For strong-coupling superconductors, *e.g.* lead, the temperature dependence of the gap is known to be raised slightly from the BCS curve in higher temperature region just below T_c. This deviation from the BCS curve is, however, very small (at most about a few percent).[40] Accordingly, our present result does not contradict to the picture that $Bi_2Sr_2CaCu_2O_8$ is a strong-coupling superconductor.

4.1.3 *Tip distance dependence of the tunneling conductance*

Figure 6 shows $dI/dV-V$ curves obtained with varying the tip distance at a fixed position of the cleaved Bi-O surface at 4.2 K.[28,29] The distance between the tip and the sample is denoted by the initial tunneling current $I_0=3$, 6, 8 and 10 nA for $V_0=150$ mV, which is far larger than the superconducting energy gap. With increasing I_0, the tip distance is reduced as described in §2.1. Each curve is normalized at $V=30$ mV. In each $dI/dV-V$ curve a sharp drop of conductance is found and dI/dV reaches to almost zero around zero bias voltage, showing the superconducting energy gap structure. However, the $dI/dV-V$ curve varies strongly with respect to the tip distance in the outside region of the gap. In the curve at $I_0=10$ nA, for which the tip distance is the smallest in the present experiment, the essential feature of the BCS density of states is reproduced as shown in Fig. 6. With increasing the tip distance the normalized differential conductance outside the gap is strongly enhanced and has a positive slope for positive

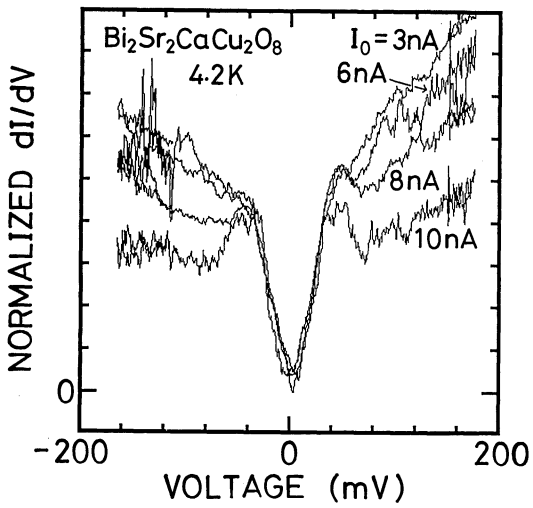

Fig. 6. $dI/dV-V$ curve for the tunneling at the cleaved surface at various tip distances at 4.2 K. The tip distance is denoted by I_0 as described in the text. Curves for $I_0=3$, 6, 8 and 10 nA at $V_0=150$ mV are shown together, normalized at 30 mV.

bias voltage. The slope becomes steeper with increasing the tip distance. On the other hand, the $dI/dV-V$ curve is rather insensitive to the tip distance at the midgap region. These behaviors are qualitatively similar to those reported by Hasegawa *et al.*[27] The differential conductance at the cleaved surface does not represent correctly the density of states of the sample.

In order to investigate whether such a phenomenon is due to the intrinsic nature of the STM measurement and check the operation of our STM apparatus, we measured $dI/dV-V$ curves for a typical conventional superconductor, lead, with varying the tip distance. Figure 7 shows $dI/dV-V$ curves of bulk lead for several different tip distances, corresponding to the initial current $I_0=5$, 7, 8 and 10 nA at $V_0=20$ mV. Each curve is drawn being shifted by one division. Although the differential conductance near zero bias voltage is slightly enhanced because of high reduced temperature $T/T_c\simeq 0.6$, the $dI/dV-V$ curve is clearly BCS like and shows no dependence of the tip distance. It was confirmed that in the STM method the differential conductance gives the electronic density of states of lead directly, irrespective of the tip distance. We have also proven the reliability of our apparatus at the same time.

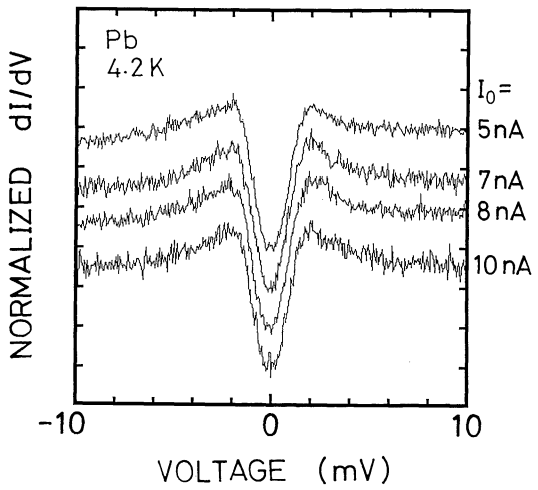

Fig. 7. $dI/dV-V$ curve for lead at various tip distances at 4.2 K. Curves for $I_0=5$, 7, 8 and 10 nA at $V_0=20$ mV are shown. The zero conductance of each curve is shifted by one division for clarity.

As discussed in §2.1, the tunneling current is given as eq. (3). The tip distance dependent $dI/dV-V$ curve shown in Fig. 6 suggests that in the tunneling at the cleaved Bi–O surface the tunneling transition matrix element M depends on the electron energy and its dependence vary with the tip distance. The energy dependence of the tunneling matrix element appears to become stronger with increasing the tip distance. The differential conductance is no longer proportional to the electronic density of states of the sample for the tunneling at the cleaved Bi–O surface. One must, therefore, discuss tunneling results at the Bi–O surface with great care, as pointed out by Hasegawa *et al.*[27] We attribute the tip distance dependent conductance curve at the cleaved surface to the structure of this material. As well as $Bi_2Sr_2CaCu_2O_8$, cuprate superconducting oxides have the layered crystal structure. For $Bi_2Sr_2CaCu_2O_8$ sheets of Ca, Cu–O, Sr–O and Bi–O are stacked alternatively. For high-T_c superconducting oxides, it is accepted that metallic electronic states, which bear the superconductivity, are confined within the Cu–O layer. Particularly, for Bi-based cuprate oxides two dimensionality of the electronic band is higher than other high-T_c oxides. The electronic behavior in the Bi–O layer is rather semiconducting. Even for the tunneling measured at the cleaved surface, the tunneling electron appears to be coming mainly from the electronic state in the Cu–O layer for low bias region, because available states are only in the Cu–O layer. The characteristic superconducting gap structure in each curve as shown in Fig. 6 well supports the above picture. In this configuration, therefore, the electron tunneling occurs through series tunneling barriers, i.e. Bi–O, Sr–O layers and the vacuum gap. The allowed electronic level is different in energy among these barriers. The width of each barrier is comparable to the inverse of the wave number of tunneling electron. The increase of the tip distance corresponds to widening of the vacuum gap. It is presumed that the energy dependence of the tunneling matrix element for the tunneling process is strongly modified by such a complicated interface barrier structure.

Muldoon *et al.*[41] have reported the electron tunneling experiment between aluminum and lead through the tunneling barrier which consists of aluminum-oxide and some kinds of organic molecules. They found that the nonlinear tunneling I-V curve is very sensitive to the kind of organic molecule and explained it by the model calculation of the tunneling current assuming the elastic tunneling through two barriers in series, which are different in height and width. Our present configuration of tunneling barrier at the Bi–O surface is similar to that of Muldoon *et al.* Our results for the tip distance dependence might be explained in terms of series tunneling barriers. It is naturally expected from such a model that the energy dependence of the transition probability is weak near zero bias voltage. It is understood from such a situation that with increasing the tip distance the normalized $dI/dV-V$ curve is varied significantly at high bias voltage region, while it is almost unchanged at low bias voltage region ($|eV|<\Delta$).

We should also point out the possibility of the inelastic scattering of electron in Bi–O or Sr–O layer. If the tunneling electron is scattered by excitations in tunneling barriers, the inelastic tunneling process becomes important. Then the $dI/dV-V$ curve is modified according to the spectra of excitations. Although the inelastic tunneling does

not explain the tip distance dependent $dI/dV-V$ curve by itself, the possibility that the inelastic electron tunneling modifies the $dI/dV-V$ curve in the present experiment, can not be excluded.

Such a property of the electron tunneling, which is sensitive to the barrier structure, may also explain existing controversial tunneling experiments for cuprate superconductors, whose $dI/dV-V$ curves show frequently so-called V-shape and are roughly similar to that. In the case of far tip distance in the present experiment. It is deduced that in these experiments the structure of the tunneling gap was not controlled microscopically, because of the layered structure of these materials. Accordingly, it is not appropriate to discuss the detailed functional shape of the density of states with such data. We present the tunneling conductance free from such ambiguity measured at the lateral surface in following sections.

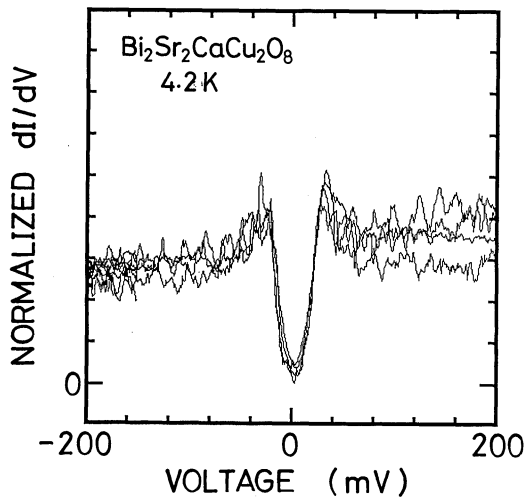

Fig. 8. $dI/dV-V$ curve for the tunneling at the lateral surface at various tip distances at 4.2 K. Curves for $I_0=2$, 4, 8 and 20 nA at $V_0=200$ mV are shown together. All curves are identical irrespective of the tip distance.

4.2 Tunneling at the lateral surface

4.2.1 Tunneling conductance without tip distance dependence

As described in §4.1.3, we could not obtain the correct electronic density of states at the cleaved surface because of the layered structure of cuprate superconductors. We expect that the electronic density of states would be obtained correctly at the lateral surface perpendicular to the cleaved surface, because in this configuration the tip and the Cu–O layer is separated only by a vacuum gap as in the case of lead. As mentioned in §3.1, the extremely clean lateral surface is rarely obtained. We carried out the tunneling spectroscopic measurement in such a lateral surface. Figure 8 shows $dI/dV-V$ curves obtained at the fixed position of the lateral surface with varying the tip distance. We investigated the $dI/dV-V$ curve at different positions, but we could not find any spatial variation of the $dI/dV-V$ curve on an atomic scale. We obtained essentially the identical curve in every measured positions. In Fig. 8, four curves for different tip distances, corresponding to the initial current $I_0=2$, 4, 8 and 20 nA at $V_0=200$ mV, are shown together, normalized at $V=25$ mV. We find that the normalized $dI/dV-V$ curve is identical irrespective of the tip distance at the entire region of applied voltage shown in Fig. 8, in contrast with the case of the cleaved surface. The differential conductance is reduced to almost zero and flat around zero bias voltage. With increasing the bias voltage, the $dI/dV-V$ curve shows a relatively sharp peak and becomes almost flat for far higher voltage. In this manner, the curve of $dI/dV-V$ measured at the lateral surface well characterizes the gap structure of superconductor.

It is expected that Cu–O, Bi–O and other layers come out periodically in the lateral surface of $Bi_2Sr_2CaCu_2O_8$. The spatial period is estimated to be larger than 1.5 nm, half length of unit distance of the *c*-axis, if we take into account the slight inclination of the lateral surface. We can accordingly approach to each layer alternatively with scanning the tip. However, we could obtain only the identical $dI/dV-V$ curve in every measured point of the lateral surface. Metallic electrons are likely confined within the Cu–O layer. In the range of voltage sweep in the present experiment, the electron tunneling occurs almost through electronic states in the Cu–O layer, because there is little available electronic level in other layers. It is deduced that even if the tip is closest to the Bi–O layer, the tunneling current flows obliquely between the Cu–O layer and

the tip metal. Under these circumstances, we could obtain only the identical $dI/dV-V$ curve irrespective of the tip position in the lateral surface.

The Cu–O layer and the tip are separated only by a vacuum gap in this configuration as in the case of lead. It is naturally expected that the tunneling matrix element is nearly independent of the electron energy. The electronic density of states for the superconducting phase in this material is, accordingly, proportional to the differential conductance observed at the lateral surface. Our obtained spectra at the lateral surface are the first data appropriate for discussions about intrinsic properties of superconductivity. The density of states obtained at the lateral surface is discussed in detail in following sections.

4.2.2 Fit of the conductance to the BCS form

Figures 9(a) and 9(b) show the typical tunneling conductance at different positions in the sample surface. The essential behavior at low energy region described below is reproduced at different positions. As shown in Figs. 9(a) and 9(b), the sharp drop of the conductance corresponding to the energy gap structure and the enhancement at the gap edge are clearly seen in the electronic density of states for the superconducting phase. The whole shape is alike the BCS density of states. The conductance near zero bias voltage is reduced to about 0.5 nS. In our measuring system the background leak of the order of 0.2 nS is usually observed. If we take into account this background leak, it is understood that the conductance vanishes and is flat near zero bias voltage within experimental errors. If we assume the conductance curve for the normal phase by a smooth interpolation from high bias voltage regions, the area of digged gap region below the interpolation curve and that of enhanced peaks above the curve are almost equal as shown by hatched areas in Fig. 9(a). The number of states is conserved for the transition from the normal to the superconducting phase. This fact assures again that $dI/dV-V$ curves obtained at the lateral surface give the correct electronic density of states unambiguously.

Here, we try to estimate the gap parameter.

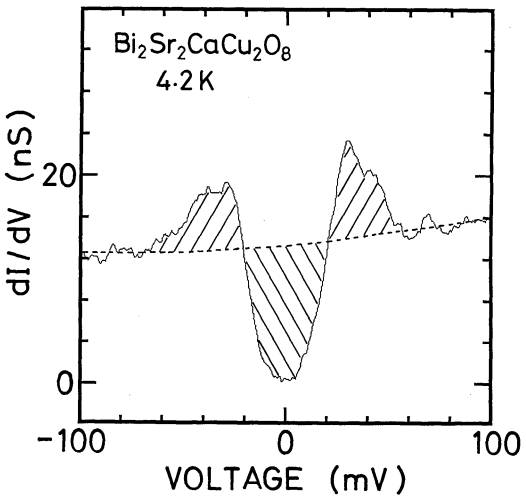

Fig. 9(a). $dI/dV-V$ curve for the tunneling at the lateral surface at 4.2 K. Four raw data are accumulated for the improvement of the signal to noise ratio. The broken curve represents the assumed normal state conductance as the smooth interpolation. The number of states is conserved between the normal and the superconducting phase, as shown by hatched areas.

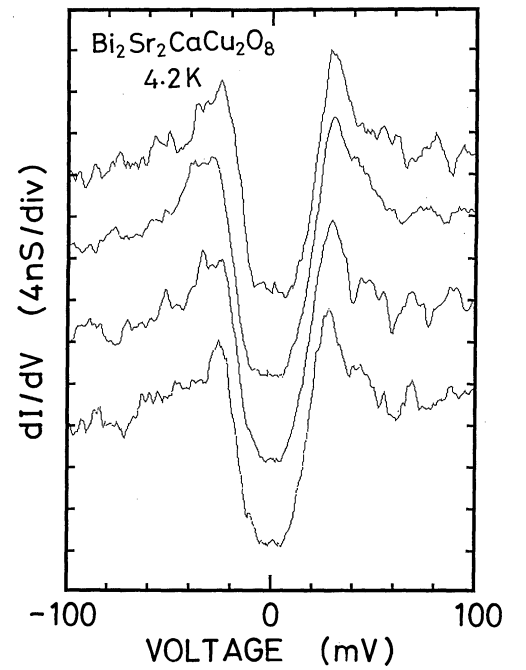

Fig. 9(b). $dI/dV-V$ curves for the tunneling at the lateral surface taken at four different positions. The zero conductance line is shifted by two divisions for clarity.

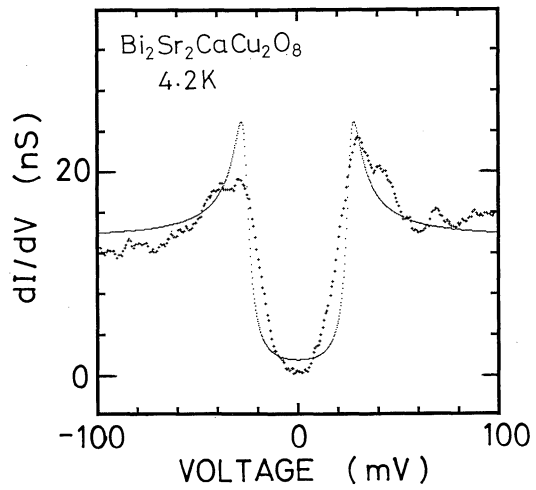

Fig. 10. Fitting of the data shown in Fig. 9(a) to the broadened BCS density of states. The thin dotted curve shows eq. (9) with $\Delta=26$ meV and $\Gamma=3$ meV.

It is apparent that the BCS curve does not give a good agreement with the present data. For better fitting, we introduce the broadening of electronic level. In order to take into account the lifetime broadening, we use the broadened BCS density of states[42] with the gap parameter Δ and the broadening parameter Γ described as

$$N_S(E)=\mathrm{Re}\left[\frac{E-i\Gamma}{\{(E-i\Gamma)^2-\Delta^2\}^{1/2}}\right]N_N, \quad (9)$$

where the electronic density of states for the normal phase N_N is supposed to be almost constant near the Fermi level. In Fig. 10, the curve of eq. (9) with $\Delta=26$ meV and $\Gamma=3$ meV is shown together with the present conductance curve. A divergence at the gap edge in the BCS density of states is smeared by a small broadening parameter Γ. However, the agreement is insufficient as shown in Fig. 10. The detailed fitting of the $dI/dV-V$ curve is discussed in the following section. Here we use eq. (9) only for the estimation of the gap parameter, which is compared with other reported values. From the fit in Fig. 10, Δ is estimated as 26 meV at 4.2 K in assuming an isotropic gap. This value of Δ at 4.2 K corresponds to $2\Delta/kT_c=7$ for $T_c=87$ K. Our present value of 7 is in agreement with reported values for $2\Delta/kT_c$ in $Bi_2Sr_2CaCu_2O_8$,[24] which are in the range 6 to 11. The value of $2\Delta/kT_c=7$ is much larger than the BCS value of 3.52 in the weak-coupling limit. It is even larger than that of well-known strong-coupling superconductors; *e.g.* $2\Delta/kT_c=4.3$ and 4.6 for Pb[13] and Hg,[43] respectively. A large value of $2\Delta/kT_c$ indicates that $Bi_2Sr_2CaCu_2O_8$ is a strong-coupling superconductor. However, the absolute magnitude of $2\Delta/kT_c$ should be discussed in connection with the gap anisotropy which is described in the following section.

4.2.3 Anisotropy of the gap

The obtained electronic density of states indicates a finite gap. However, it can not be fitted by the BCS density of states, in which an isotropic gap is assumed. Such a disagreement would be explained by an anisotropy of the gap. We discuss the shape of the $dI/dV-V$ curve from the view point of an anisotropic gap below. In the case of isotropic superconducting gap, the constant gap parameter Δ gives the BCS density of states. On the other hand, in the anisotropic gap case, the amplitude of Δ varies in $\boldsymbol{k}$-space. As a result, finite density of states appears at midgap region. We consider two kinds of anisotropic gaps; one is the case in which Δ vanishes somewhere in $\boldsymbol{k}$-space and another is the non-vanishing case.

Before investigating individual models, we define the gap density function $D(\Delta)$. The electronic density of states $N(E)$ is generally given as

$$N(E)=\sum_{\boldsymbol{k}}\delta(E-E(\boldsymbol{k})), \quad (10)$$

where $E(\boldsymbol{k})$ is the quasi-particle energy and described as

$$E(\boldsymbol{k})=(\varepsilon_k^2+\Delta^2(\boldsymbol{k}))^{1/2}, \quad (11)$$

where ε_k is the one-electron energy at the normal phase measured from the Fermi energy. Equation (10) is rewritten as

$$N(E)\propto\int d\Delta'\int dk\, d\Omega k^2\delta(E-(\varepsilon_k^2+\Delta'^2)^{1/2})\delta(\Delta'-\Delta(\boldsymbol{k})), \quad (12)$$

where the k-summation is replaced by the integral over $k=|k|$ and its solid angle Ω and an unimportant numerical factor is ignored in the equation. The precise energy dependence of $N(E)$ depends on both the band dispersion and k-dependent $\Delta(k)$. For the sake of simplicity, we assume that the band dispersion is isotropic and Δ depends only on the direction in k-space. Such a simplification does not change the essential property discussed below. The integral over Ω can be performed independently. The gap density function $D(\Delta')$ is defined as

$$A\int d\Omega\,\delta(\Delta'-\Delta(k))\equiv D(\Delta'). \tag{13}$$

The numerical factor A is chosen as satisfying the following normalization condition as

$$\int D(\Delta')\,d\Delta'=1. \tag{14}$$

After the integral over k, assuming the moderate dispersion, we obtain the BCS form as

$$\int dk\,k^2\delta(E-(\varepsilon_k^2+\Delta'^2)^{1/2})\propto\frac{E}{(E^2-\Delta'^2)^{1/2}}N(0), \tag{15}$$

where $N(0)$ denotes the density of states at the Fermi level for the normal phase. After all, the density of states is written as

$$\frac{N(E)}{N(0)}=\int D(\Delta)\frac{E}{(E^2-\Delta^2)^{1/2}}d\Delta, \tag{16}$$

where the prime is omitted without confusion. Although there are several calculations of the electronic density of states for an anisotropic gap,[39,44] we discuss our results on the above simple model. Because of the simplification, eq. (16) reveals the essential behavior only at low energy region.

First we discuss the case in which Δ vanishes somewhere on the Fermi surface. As described in §1, the pair wave function of high-T_c superconductor is of the spin singlet state. Therefore, the orbital part of the pair wave function must be of even parity. Then the s and d-wave paring are candidates and the p-wave paring is not allowed. Most simply, the gap anisotropy could be originated from the d-wave paring. It is well established that the superconductivity occurs in the nearly square lattice of the Cu–O layer. Accordingly, the mixing of different d-waves is energetically unfavorable. As a result, the gap with d-wave symmetry can vanish along lines on the Fermi surface, as far as we consider the on-site and the nearest neighbor interaction. The gap with point nodes expected from the mixture of two d-waves is excluded.

We examine the line nodes model, where Δ is described as

$$\Delta=\Delta_0\cos 2\phi, \tag{17}$$

where Δ_0 is the maximum value of Δ and ϕ is the azimuth. Here, Δ depends only on ϕ and vanishes along lines $\phi=\pi/4$, $3\pi/4$, $5\pi/4$ and $7\pi/4$. According to eq. (13), $D(\Delta)$ is calculated for $|\Delta|<\Delta_0$ as

$$D(\Delta)=-\frac{4}{\pi}\left(\frac{\partial\Delta}{\partial\phi}\right)^{-1}_{\Delta=\Delta_0\cos 2\phi}. \tag{18}$$

As a result, $D(\Delta)$ is obtained as

$$D(\Delta)=\begin{cases}\dfrac{2}{\pi(\Delta_0^2-\Delta^2)^{1/2}} & \text{for } |\Delta|<\Delta_0\\ 0 & \text{for } |\Delta|>\Delta_0.\end{cases} \tag{19}$$

Substituting this in eq. (16),

$$\frac{N(E)}{N(0)}=E\int_0^E\frac{2}{\pi(\Delta_0^2-\Delta^2)^{1/2}}\frac{1}{(E^2-\Delta^2)^{1/2}}d\Delta. \tag{20}$$

For low energy region,

$$\frac{N(E)}{N(0)}\propto\frac{E}{\Delta_0}. \tag{21}$$

This relation gives the general feature of the gap with line nodes Δ, where the electronic density of states is proportional to E for low energy.

As discussed in §2.1, for the tunneling process in the STM method the wave number is not conserved because the area through which the tunneling occurs is restricted at most few

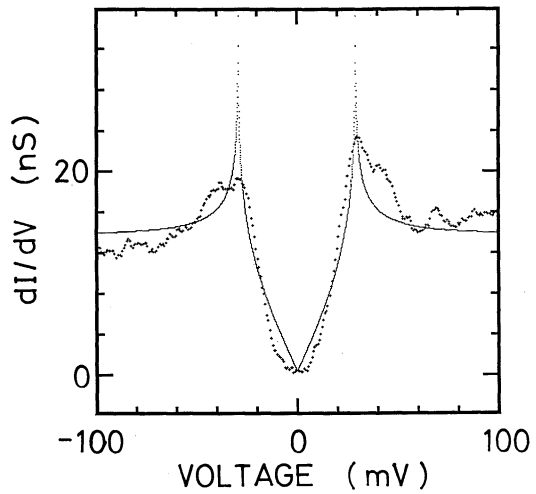

Fig. 11. Fitting of the data shown in Fig. 9(a) to the line nodes model. The thin dotted curve shows the density of states for the line nodes model described as eq. (20) with $\Delta_0=29$ meV.

atoms. No matter which direction against the crystalline axis the tunneling occurs, every wave number components contribute to the tunneling conductance. Therefore, we can properly compare the tunneling result with the total density of states $N(E)$ calculated above. It is obvious that the line nodes model does not agree with the present data as shown in Fig. 11. It does not explain the flat conductance at low energy region in the present data. It is natural if one remember that the gap with line nodes gives linear density of states to energy. It is clear that the pairing with the pure d-wave symmetry is not formed in this superconductivity.

Next we consider the case of the anisotropic gap where Δ depends on $\boldsymbol{k}$ but is finite everywhere on the Fermi surface. We introduce the rectangular gap density function $D(\Delta)$ as,

$$D(\Delta)=\begin{cases}\dfrac{1}{\Delta_{\max}-\Delta_{\min}} & \text{for } \Delta_{\min}\leqq|\Delta|\leqq\Delta_{\max}\\ 0 & \text{for } 0\leqq|\Delta|<\Delta_{\min},\ |\Delta|>\Delta_{\max},\end{cases} \tag{22}$$

where $\Delta_{\min}$ and $\Delta_{\max}$ denote minimum and maximum of the positive gap value, respectively. The mean value of Δ_1 is given by $\Delta_1=(\Delta_{\min}+\Delta_{\max})/2$. The half of the width is given by $W=(\Delta_{\max}-\Delta_{\min})/2$. This width is coming from the anisotropic gap dependent on the direction in $\boldsymbol{k}$-space.

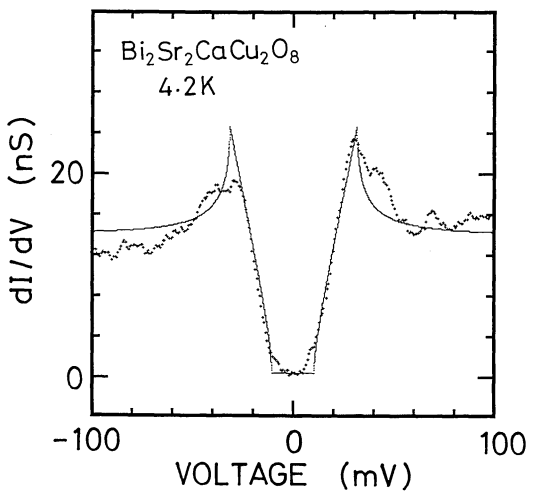

Fig. 12. Fitting of the data shown in Fig. 9(a) to the model of rectangular $D(\Delta)$. The thin dotted curve shows the density of states described as eqs. (16) and (22) with $\Delta_1=21$ meV and $W=0.5\,\Delta_1$.

In Fig. 12, the fit by the present model with $\Delta_1=21$ meV and $W=0.5\Delta_1$ is shown together with the experimental result. The flat bottom near zero bias voltage is satisfactorily reproduced by the present model of the anisotropic gap. This indicates that in the superconducting phase of this material the gap is finite everywhere on the Fermi surface, while a considerable anisotropy of the gap also exist. The symmetry of the gap is discussed in §5.

The minimum value of the gap is estimated as $\Delta_1-W\simeq 10$ meV from the fitting. The mean value Δ_1 is obtained as $\Delta_1=21$ meV and corresponds to $2\Delta_1/kT_c=5.6$. The value of $2\Delta_1/kT_c=5.6$ suggests again that $Bi_2Sr_2CaCu_2O_8$ is a strong-coupling superconductor, although it is not obvious which Δ value should be used in such an anisotropic gap case.

4.3 *Temperature dependence of the magnetic field penetration depth*

Figure 13 shows the temperature dependence of the real part χ' of AC susceptibility $\chi=\chi'+i\chi''$ of the sample with a dimension of $0.85\times2.6\times0.076\,mm^3$. The value of χ' is calibrated by the perfect diamagnetism of similar shaped lead thin plate measured at 1.3 K, in which the magnetic field penetration is negligible because of the short penetration depth $\lambda(0)=39$ nm.[45] Owing to the error in measuring the thickness of the sample, the absolute value of χ' contains relatively large error about 10–20% and λ as well. However, we are interested only in the temperature dependence not in the absolute magnitude of λ. As shown in Fig. 13, $-4\chi'(T)$ is almost constant at low temperature and gradually decreases with increasing temperature. It rapidly decreases near T_c and vanishes at 89 K, which is roughly equal to $T_c=87$ K determined from the midpoint of resistive transition. The imaginary part χ'' is detectable only below a few kelvin from 89 K. Almost full Meissner fraction is observed at 4.2 K. This indicates that the present sample undergoes a bulk superconducting transition.

In Fig. 14, $\lambda(T)-\lambda(4.2\,K)$, which is led from $\chi'(T)$ shown in Fig. 13, is plotted as a function of $(T/T_c)^2$. Here, we assumed that the field penetration is dominant in the perpendicular direction to the plate. However, the field penetration along to the *a-b* plane can not be excluded, because of the high two dimensionality in electronic states of this material. Owing to this ambiguity, we do not discuss the absolute magnitude of λ but only its temperature dependence, which represents the essential feature of the superconducting phase and is independent of the direction of the field penetration. The theoretical curve of the BCS dirty local limit λ_{eff} described as,

$$\frac{\lambda_{eff}(T)}{\lambda_{eff}(0)}=\left[\frac{\Delta(T)}{\Delta(0)}\tanh\frac{\Delta(T)}{2kT}\right]^{-1/2}, \qquad (23)$$

with fitting parameter $\lambda(0)=4\,\mu m$ is also shown together in the figure. Here we assume that $\Delta(T)$ follows the BCS prediction with $\Delta(0)=1.76\,kT_c=14$ meV of the BCS weak-coupling limit. In whole temperature region, observed $\lambda(T)$ is almost consistent with the dirty local limit. We are interested in the temperature dependence of λ at low temperature region where the low energy excitation is well reflected. Figure 15 shows enlarged $\lambda(T)-\lambda(4.2\,K)$ versus $(T/T_c)^2$ in low temperature region. The dirty local limit with $\lambda(0)=6\,\mu m$ and $\Delta(0)=14$ meV gives a better fit in low temperature region as shown in the figure. The temperature dependence of $\lambda(T)-\lambda(4.2\,K)$

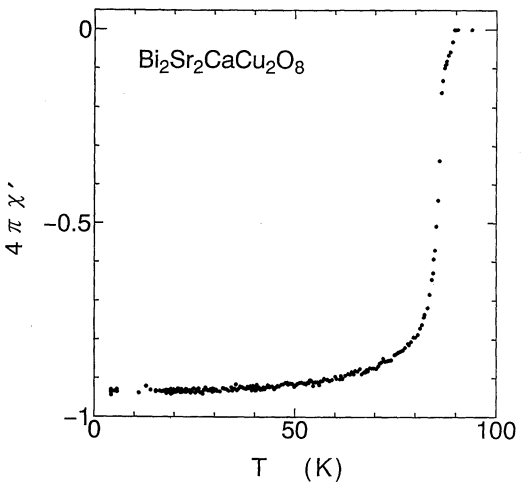

Fig. 13. Temperature dependence of the real part χ' of AC susceptibility of a single crystal of $Bi_2Sr_2CaCu_2O_8$.

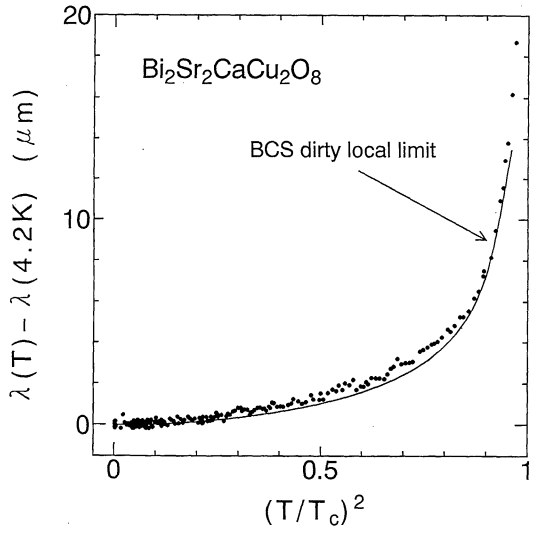

Fig. 14. Temperature dependence of the penetration depth $\lambda(T)-\lambda(4.2\,K)$ as a function of $(T/T_c)^2$. The solid curve represents the BCS dirty local limit described as eq. (23) with $\lambda(0)=4\,\mu m$.

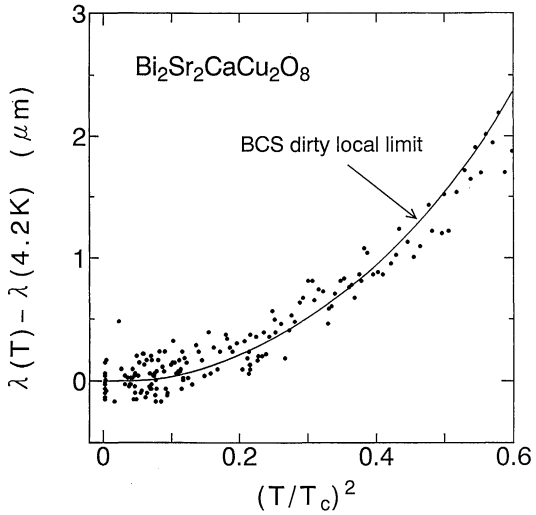

Fig. 15. Enlargement of Fig. 14 at low temperature. The solid curve represents the BCS dirty local limit described as eq. (23) with $\lambda(0)=6\,\mu$m.

does not have any finite slope at low temperature region. The temperature dependence of $\lambda(T)-\lambda(4.2\text{ K})$ is described by the thermal activated behavior not by the power law. This fact indicates the finite gap on the Fermi surface and reconfirms the result of the tunneling spectroscopy discussed in §4.2.3. The gap value $\Delta(0)=14$ meV estimated from the fitting, is consistent with the minimum gap value of $\Delta_1-W\simeq 10$ meV obtained by the tunneling measurement described in §4.2.3.

Our present result is consistent with that obtained by Harshman *et al.*[34] on the single crystal of $Bi_2Sr_2CaCu_2O_8$ by the μSR measurement. Maeda *et al.*[32] reported that $\lambda(T)-\lambda(0)$, measured by the rf-resonance method, exhibits T^2 dependence in $Bi_2Sr_2CaCu_2O_8$. We do not know the source of such T^2 dependence. We only deduce that the T^2 dependence observed by Maeda *et al.* is originated from other mechanism than the anisotropic gap with nodes. Our result is also consistent with those on single crystals of $YBa_2Cu_3O_7$[11] by the low-field DC magnetization measurement and thin film of $YBa_2Cu_3O_7$[30] by the AC inductance method. It is interesting that the same result is obtained commonly among different materials. It is understood to be the intrinsic nature in high-T_c cuprate superconductors that the gap is finite on the Fermi surface.

§5. Symmetry of the Pair Wave Function

Our tunneling spectroscopic measurement described in §4.2 shows that the gap is finite everywhere on the Fermi surface while the considerable gap anisotropy exists at the same time. The temperature dependence of the penetration depth described in §4.3 reinforces the finite gap. These experimental results indicate that the symmetry in the pair wave function is predominantly of the isotropic *s*-wave. However, these are not explained only by the isotropic *s*-wave, because our tunneling result clearly shows an anisotropy of the gap. It is understood that the attractive interaction is not given only by the on-site interaction. We need to introduce the extended interaction. If we consider the small distortion of the square lattice, we cannot distinguish rigorously the *s*-wave from the *d*-wave. However, it is still important for the clarification of the origin of superconductivity to specify the pairing symmetry in the nearly square lattice. The extended *s*-wave could give the gap anisotropy. Most simply, the gap is described for the extended *s*-wave in the square lattice with the lattice constant a as,

$$\Delta(\boldsymbol{k})=\Delta_0+\Delta_1(\cos(k_x a)+\cos(k_y a)) \quad (24)$$

where Δ_0 is the isotropic gap component and Δ_1 is the amplitude of additional anisotropic term coming from the nearest neighbor interaction. Although the gap is $\boldsymbol{k}$-dependent as represented by eq. (24), the estimated gap anisotropy does not become large, because the electronic band dispersion for the square lattice has the same $\boldsymbol{k}$-dependence as the anisotropic component of Δ in the lowest order. It is difficult to explain the observed large anisotropy only by the extended *s*-wave. Accordingly, our present result suggests the contribution of *d*-wave component in the pair wave function. It is deduced that the pair wave function has the symmetry of the mixture of *s* and *d*-wave. However, it is open problem how the *s*-wave can be mixed with a considerable amount of *d*-wave in the nearly square lattice.

Shen *et al.*[46] performed angle-resolved photoemission spectroscopy (ARPES) on single crystals of $Bi_2Sr_2CaCu_2O_8$ and obtained spectra at various points in the Brillouin zone.

They observed k dependent gap parameter and claimed that the gap disappears along Γ-Y direction. Their result is qualitatively consistent with our tunneling result with respect to the gap anisotropy. However, the resolution of the photoemission spectroscopic experiment is not enough to determine a small gap precisely. Our result that the gap is finite over whole Fermi surface is more reliable, because the tunneling experiment has a sufficient resolution. The NMR Knight shift, which is sensitive to the quasi-particle excitation at low energy region, was measured by Barret *et al.*[47] It was reported that the temperature dependence of the Knight shift was presumably explained by the *s*-wave pairing, although they pointed out the possibility of the *d*-wave pairing at the same time. The temperature dependence of the nuclear relaxation rate $1/T_1$[48] showed no coherence peak and was not thermally activation type in low temperature. These behaviors were discussed by the *d*-wave pairing. However, Koyama *et al.*[49] reported that even if the *s*-wave symmetry is assumed, the spin fluctuation due to the strong correlation effect of electron scatters quasi-particle. As a consequence the enhancement of $1/T_1$ just below T_c is suppressed. The absence of the coherence peak of the nuclear relaxation rate does not exclude the *s*-wave pairing. Moreover, non-thermally activation behavior of $1/T_1$ does not necessarily indicate the gap with nodes, because extra relaxation mechanisms, *e.g.* due to magnetic impurities, can easily smear the thermally activation behavior in low temperature. Accordingly, these results obtained by other experiments are not inconsistent with our present conclusion that the symmetry of the pair wave function is the mixture of *s* and *d*-wave. Kotliar[50] discussed that in the mixed order parameter of *s* and *d*-wave, if the relative phase between *s* and *d*-wave order parameter is chosen as $\pi/2$, i.e. $s+id$, the order parameter do not vanish. Such a pairing is also possible from our present result.

In high-T_c superconductors, it is accepted that the on-site Coulomb interaction in the Cu–O layer is fairly large.[5] Therefore, it is suspected that the on-site attractive force between electrons does not become large enough to mediate the electron pairing in such a strong correlation system. However, our present result indicates that the attractive interaction in cuprate high-T_c superconductors has large isotropic component. Naively, the isotropic attractive interaction is the on-site one. It is still open problem how the on-site attractive force overcome the strong correlation. On the other hand, our present result of the anisotropic gap shows a considerable *d*-wave component in the pair wave function. The attractive force between electrons is not only due to the on-site interaction, but also the extended one.

§6. Summary

The electron tunneling study was performed on $Bi_2Sr_2CaCu_2O_8$ with use of the STM. Both the cleaved and lateral surface of single crystal were investigated. For the tunneling at the cleaved surface, the spatial variation of the gap parameter was found. The tip distance dependent conductance curve was obtained and attributed to the tunneling gap structure coming from the layered crystal structure of cuprate high-T_c oxides. The tunneling conductance at the cleaved surface is no longer proportional to the electronic density of states. On the other hand, for the tunneling at the lateral surface we succeeded to obtain the correct electronic density of states. From the shape of the conductance curve, it is understood that the gap is finite everywhere on the Fermi surface and its minimum value is estimated as $\Delta_{min} \simeq 10$ meV while the gap has a considerable anisotropy. The temperature dependence of the penetration depth $\lambda(T)$ was also obtained. It showed the behavior of thermal activation type indicating the finite gap on the Fermi surface. This reconfirms the tunneling result. The gap value estimated from $\lambda(T)$ is almost consistent with the minimum value obtained from the tunneling spectroscopy.

Completely opened gap indicates a large *s*-wave component in the pair wave function. Superconductivity in cuprate high-T_c superconductors is mainly brought about by the isotropic attractive interaction between electrons. On the other hand, the anisotropy of gap shows a considerable contribution of *d*-wave. It is deduced that the symmetry of the pair wave function is the mixture of *s* and *d*-wave. The attractive force which forms the

electron pair is not only due to the on-site attractive interaction, but also the extended one.

Acknowledgements

We would like to thank Professor T. Sambongi for valuable discussions and useful advices. We also would like to thank Professor F. J. Ohkawa for valuable discussions. We also would like to thank Professor F. Minami of Tokyo Institute of Technology and Dr. S. Takekawa of National Institute for Research in Inorganic Materials for providing $Bi_2Sr_2CaCu_2O_8$ sample. We also would like to thank Dr. A. Yamanaka for discussion and helpful advice on the property of the single crystal sample. We are also indebted to Dr. T. Okada and Dr. T. Takase of Olympus Optical Co., Ltd., for their useful advices on STM apparatus. This work was supported in part by Grant-in-Aid for Scientific Research on Priority Area, "Science of High-T_c Superconductivity" given by Ministry of Education, Science and Culture.

References

1) G. Bednorz and K. A. Müller: Z. Phys. **B64** (1986) 189.
2) J. Bardeen, L. N. Cooper and J. R. Schrieffer: Phys. Rev. **108** (1957) 1175.
3) W. L. McMillan: Phys. Rev. **167** (1968) 331.
4) M. Takigawa, P. C. Hammel, R. H. Heffner and Z. Fisk: Phys. Rev. **B39** (1989) 7371.
5) A. Fujimori, E. Takayama-Muromachi, Y. Uchida and B. Okai: Phys. Rev. **B35** (1987) 8814.
6) N. Nücker, J. Fink, J. C. Fuggle, P. J. Durham and W. M. Temmerman: Phys. Rev. **B37** (1987) 5158.
7) M. B. Maple, J. W. Chen, Y. Dalichaouch, T. Kohara, C. Rossel and M. S. Torikachvili: Phys. Rev. Lett. **56** (1986) 185.
8) D. E. MacLaughlin, C. Tien, W. G. Clark, M. D. Lan, Z. Fisk, J. L. Smith and H. R. Ott: Phys. Rev. Lett. **53** (1984) 1833.
9) F. Gross, B. S. Chandrasekhar, D. Einzel, K. Andres, P. J. Hirschfeld, H. R. Ott, J. Beuers, A. Fisk and J. L. Smith: Z. Phys. **B64** (1986) 175.
10) W. W. Warren, Jr., R. E. Walstedt, G. F. Brennert, G. P. Espinosa and J. P. Remeika: Phys. Rev. Lett. **59** (1987) 1860.
11) A. T. Fiory, A. F. Hebard, P. M. Mankiewich and R. E. Howard: Phys. Rev. Lett. **61** (1988) 1419.
12) I. Giaever: Phys. Rev. Lett. **5** (1960) 147.
13) I. Giaever, H. R. Hart, Jr. and K. Megerle: Phys. Rev. **126** (1962) 941.
14) G. Binnig, H. Rohrer, Ch. Gerber and E. Weibel: Phys. Rev. Lett. **49** (1982) 57.
15) R. V. Coleman, B. Drake, P. K. Hansma and G. Slough: Phys. Rev. Lett. **55** (1985) 394.
16) K. Nomura and K. Ichimura: Solid State Commun. **71** (1989) 149.
17) H. F. Hess, R. B. Robinson, R. C. Dynes, J. M. Valles, Jr. and J. V. Waszczac: Phys. Rev. Lett. **62** (1989) 214.
18) J. Moreland, A. F. Clark, L. F. Goodrich, H. C. Ku and R. N. Shelton: Phys. Rev. **B35** (1987) 8711.
19) J. M. Valles, Jr., R. C. Dynes, A. M. Cucolo, M. Curvitch, L. F. Schneemeyer, J. P. Garno and J. V. Waszczak: Phys. Rev. **B44** (1991) 11986.
20) T. Ekino and J. Akimitsu: Phys. Rev. **B40** (1989) 7364.
21) S. Vieira, J. G. Rodrigo, M. A. Ramos, K. V. Rao and Y. Makino: Phys. Rev. **B40** (1989) 11403.
22) H. Ikuta, A. Maeda, K. Uchinokura and S. Tanaka: Jpn. J. Appl. Phys. **27** (1988) L1038.
23) S. Vieira, M. A. Ramos, M. Vallet-Regi and J. M. Gonzalez-Calbet: Phys. Rev. **B38** (1988) 9295.
24) T. Ekino and J. Akimitsu: Phys. Rev. **B40** (1989) 6902.
25) N. Miyakawa, D. Shimada, T. Kido and N. Tsuda: J. Phys. Soc. Jpn. **59** (1990) 2473.
26) K. Ichimura, K. Nomura, F. Minami and S. Takekawa: J. Phys.: Condens. Matter, **2** (1990) 9961.
27) T. Hasegawa, M. Nantoh and K. Kitazawa: Jpn. J. Appl. Phys. **30** (1991) L276.
28) K. Ichimura, K. Nomura, F. Minami and S. Takekawa: Physica C **185–189** (1991) 941.
29) K. Ichimura, K. Nomura, F. Minami and S. Takekawa: Solid State Commun. **82** (1992) 171.
30) L. Krusin-Elbaum, R. L. Greene, F. Holtzberg, A. P. Malozemoff and Y. Yeshurun: Phys. Rev. Lett. **62** (1989) 217.
31) W. Kritscha, F. M. Sauerzopf, H. W. Weber, G. W. Crabtree, Y. C. Chang and P. Z. Jiang: Physica C **179** (1991) 59.
32) A. Maeda, T. Shibauchi, N. Kondo, K. Uchinokura and M. Kobayashi: Phys. Rev. **B46** (1992) 14234.
33) Y. J. Uemura, V. J. Emery, A. R. Moodenbaugh, M. Suenaga, D. C. Johnston, A. J. Jacobson, J. T. Lewandowski, J. H. Brewer, R. F. Kiefl, S. R. Kreitzman, G. M. Luke, T. Riseman, C. E. Stronach, W. J. Kossler, J. R. Kempton, X. H. Yu, D. Opie and H. E. Schone: Phys. Rev. **B38** (1988) 909.
34) D. R. Harshman, R. N. Kleiman, M. Inui, G. P. Espinosa, D. B. Mitzi, A. Kapitulnik, T. Pfiz and D. Ll. Williams: Phys. Rev. Lett. **67** (1991) 3152.
35) P. Bordet, J. J. Capponi, C. Chaillout, J. Chenavas, A. W. Hewat, E. A. Hewat, J. H. Hodeau, M. Marezio, J. L. Tholence and D. Tranqui: Physica C **156** (1988) 189.
36) S. Takekawa, H. Nozaki, A. Umezono, K. Kosuda and M. Kobayashi: J. Cryst. Growth **92** (1988) 677.
37) A. Yamanaka: private communication; A. Yamanaka, H. Takato, F. Minami, K. Inoue and S. Takekawa: Physica C **185–189** (1991) 1027.
38) Y. Hidaka and T. Murakami: Solid State Phys. **23** (1988) 743 [in Japanese].

39) F. J. Ohkawa: J. Phys. Soc. Jpn. **56** (1987) 2267.
40) R. F. Gasparovic, B. N. Taylor and R. E. Eck: Solid State Commun. **4** (1966) 59.
41) M. F. Muldoon, R. A. Dragoset and R. V. Coleman: Phys. Rev. B**20** (1979) 416.
42) R. C. Dynes, V. Narayanamurti and J. P. Garno: Phys. Rev. Lett. **41** (1978) 1509.
43) S. Bermon and D. M. Ginsberg: Phys. Rev. **135** (1964) A306.
44) H. Ebisawa, Y. Isawa and S. Maekawa: Jpn. J. Appl. Phys. **26** (1987) L992.
45) J. M. Lock: Proc. Roy. Soc. A**208** (1951) 391.
46) Z. X. Shen, D. S. Dessau, B. O. Wells, D. M. King, W. E. Spicer, A. J. Arko, D. Marshall, L. W. Lombardo, A. Kapitulnik, P. Dickinson, S. Doniach, J. DiCarlo, A. G. Loeser and C. H. Park: Phys. Rev. Lett. **70** (1993) 1553.
47) S. E. Barret, D. J. Durand, C. H. Pennington, C. P. Slichter, T. A. Friedmann, J. P. Rice and D. M. Ginsberg: Phys. Rev. B**41** (1990) 6283.
48) P. C. Hammel, M. Takigawa, R. H. Heffner, Z. Fisk and K. C. Ott: Phys. Rev. Lett. **63** (1989) 1992.
49) T. Koyama and M. Tachiki: Phys. Rev. B**39** (1989) 2279.
50) G. Kotliar: Phys. Rev. B**37** (1988) 3664.